Quantifying reversible nitrogenous ligand binding to Co(II) porphyrin receptors at the solution/solid interface and in solution†

Kristen N. Johnson, K W Hipps*, Ursula Mazur*

Department of Chemistry and Materials Science and Engineering Program, Washington State University, Pullman, Washington, 99164-4630, United States

ABSTRACT: We present a quantitative study comparing the binding of 4-methoxypyridine, MeOPy, ligand to Co(II)octaethylporphyrin, CoOEP, at the phenyloctane/HOPG interface and in toluene solution. Scanning tunneling microscopy (STM) was used to study the ligand binding to the porphyrin receptors adsorbed on graphite. Electronic spectroscopy was employed for examining this process in fluid solution. The on surface coordination reaction was completely reversible and followed a simple Langmuir adsorption isotherm. Ligand affinities (or ΔG) for the binding processes in the two different chemical environments were determined from the respective equilibrium constants. The free energy value of −13.0±0.3 kJ/mol for the ligation reaction of MeOPy to CoOEP at the solution/HOPG interface is less negative than the ΔG for cobalt porphyrin complexed to the ligand in solution, −16.8±0.2 kJ/mole. This result indicates that the MeOPy−CoOEP complex is more stable in solution than on the surface. Additional thermodynamic values for the formation of the surface ligated species (ΔH_c = −50 kJ/mol and ΔS_c = −120 J/mol) were extracted from temperature dependent STM measurements. Density functional computational methods were also employed to explore the energetics of both the solution and surface reactions. At high concentrations of MeOPy the monolayer was observed to be stripped from the surface. Computational results indicate that this is not because of a reduction in adsorption energy of the MeOPy−CoOEP complex. Nearest neighbor analysis of the MeOPy−CoOEP in the STM images revealed positive cooperative ligand binding behavior. Our studies bring new insights to the general principles of affinity and cooperativity in the ligand−receptor interactions at the solution/solid interface. Future applications of STM will pave the way for new strategies designing highly functional multisite receptor systems for sensing, catalysis, and pharmacological applications.

INTRODUCTION

Many biological systems contain metalloporphyrin binding sites that function as receptors that can regulate reversible ligand binding in order to perform tasks like respiration, photosynthesis, metal sequestration, transfer electrons, preform enzymatic catalysis and recognize target molecules.[1-3] Duplication of this behavior in artificial porphyrin systems is desirable for the a wide range of application such as separating gas mixtures,[4] energy storage and delivery,[5,6] selective chemical sensing,[7] cancer therapeutics,[8,9] and catalysis.[10,11] In both biology and technological applications, understanding how the ligands and receptors communicate requires that these interactions be quantified.[12,13] This objective can be realized by carrying out investigations determining both ligand affinity and cooperativity through model binding experiments. Affinity denotes the strength of interaction between the ligand and the receptor. Cooperativity (synergism or allostery) occurs when the binding of one molecule to a receptor enhances (or weakens) the binding of other ligands to adjacent receptors.

Various techniques exist for characterizing ligand binding interactions and the resulting complexes at the ensemble level including electronic spectroscopy, electrochemistry, electron paramagnetic resonance and nuclear magnetic resonance spectroscopy and surface plasmon resonance. Direct molecular scale level chemical reaction monitoring methods (like

scanning tunneling microscopy, STM), however, offer the advantage of delivering more definitive mechanistic insights that are ordinarily hidden in ensemble level techniques.[14-20] STM allows simultaneous access to spatial, temporal, and intra– and intermolecular reaction dynamics in different physical environments. Publications, albeit only a few at present, demonstrated that the solution/solid interface is an effective platform for probing reversible ligand binding to porphyrin receptor events to acquire both qualitative and quantitative information about binding affinity, reaction equilibrium kinetics, thermodynamics and cooperativity.[21-31] These works include binding studies of biologically and chemically relevant species such as O_2 and nitrogen bases to porphyrin receptors substituted with first row transition metal elements supported on highly oriented pyrolytic graphite (HOPG), gold and silver substrates.[22,24,26-29] (Electrochemical STM ligand binding studies are not considered here.)

Quantitative STM studies of molecular oxygen binding affinity to CoOEP at the phenyloctane/HOPG interface, demonstrated that while the O_2–CoOEP complex is not detected in solution, it is stable at room temperature when supported on HOPG.[22] Although studies of oxygen binding and oxidation reactions of manganese porphyrins on HOPG,[21] Ag(111)[29] and Au(111)[30] in solution did not provide quantitative affinity data, they did report cooperative binding and reaction of adjacent porphyrins to oxygen.

ZnTDP, Zn(II) 5,10,15,20-*meso*-tetradodecyl porphyrin, adsorbed on graphite, was found to coordinate 3-nitropyridine more effectively than in fluid tetradecane solution.[27] Imidazole, Im, reversibly coordinated to NiOEP supported on HOPG but not to the porphyrin receptors dissolved in solution.[24]

Notable findings that emerged from the above reports are that (1) metalloporphyrins do not necessarily share the same ligand binding affinity on conducting surfaces and in solution and (2) enhanced binding of the axial ligands to surface supported porphyrin receptors is mediated by the substrate.

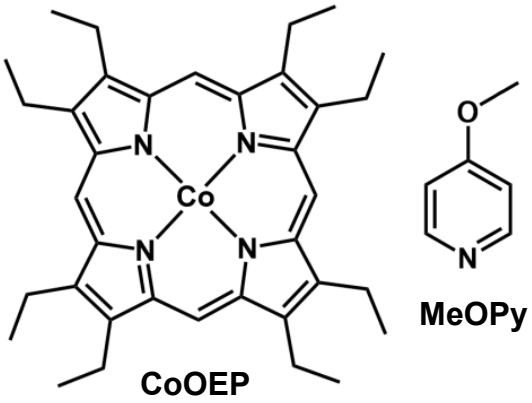

Figure 1. Molecular models of cobalt(II)octaethyl porphyrin (CoOEP) and 4-methoxypyridine (MeOPy) molecules.

We are concerned with conducting STM experiments that quantitatively examine the binding affinity of ligands to metalloporphyrins at the solution/solid interface. Concurrently, we probe for existence of cooperativity or electronic communication between the substrate and the adsorbed porphyrins that may influence the receptors' affinity toward ligands. In the report that follows we present a case study of 4-methoxy pyridine, MeOPy, ligation to CoOEP at the solution/solid interface and in solution. The binding of nitrogenous bases to Co(II) porphyrins in solution is well known[32-35] and has been exploited in molecular recognition, chemical sensing and catalytic functions as well as for the synthesizing new types of porphyrin chelates and supramolecular structures.[11,36-39] The binding of nitrogenous ligands to Co(II) porphyrins at the solution/solid interface has not been previously investigated. The MeOPy was chosen for this study because the ligand's electron donating *para*-methoxy group is expected to increase the ligand–porphyrin complex stability and minimize steric effects.

Imaging is used to follow the dynamics of MeOPy binding to HOPG surface supported CoOEP in phenyloctane (Figure 1). Electronic spectroscopy was employed for binding reaction

analysis in fluid toluene solution. In both experimental approaches, the respective ligand affinities (ΔG) were determined from the corresponding equilibrium constants. Temperature dependent STM studies yielded additional thermodynamic values. Associated theoretical calculations of the thermodynamic parameters provide comparison with the experimental values. Using the experimental distribution of MeOPy–CoOEP at the solution/solid interface and we demonstrate the existence of positive cooperativity in MeOPy binding to CoOEP.

EXPERIMENTAL SECTION

Materials: 2,3,7,8,12,13,17,18-Octaethyl-21H,23H-porphine cobalt(II) [CoOEP] and 4-methoxypryidine (MeOPy) were purchased from Aldrich. Phenyloctane (99%) was acquired from TCI Organics. Toluene (99.7%) was obtained from JT Baker. All reagents were used without further purification. Highly ordered pyrolytic graphite (HOPG) substrates, 1 cm^2, ZYA grade were purchased from Tips Nano.

Scanning Tunneling Microscopy: In all STM experiments a freshly cleaved HOPG surface was affixed in a Teflon solution cell (maximum volume 100 μL). The substrate was in contact with a either a variable temperature hot stage or a 1X Peltier heating/cooling stage outfitted with a Lakeshore 330 temperature controller with a range of −10 to 150 °C. A calibrated platinum resistance thermometer was used to monitor the temperature. The entire STM experiment was housed in an environmental chamber outfitted with gas inlets and outlets. All experiments were performed under argon. This set-up was described previously.[28]

Images were recorded using a Molecular Imaging (currently Keysight) Pico 5 STM equipped with a 1 μm^2 scanner. STM tips were made by mechanically cutting $Pt_{0.8}Ir_{0.2}$ wire (California Fine Wire Company Grover Beach, Ca.).

Electronic Spectroscopy: Solution phase ligand binding studies were carried out using a Thermo Scientific Evolution 260 Bio UV-Visible spectrophotometer with 1 cm path length quartz cuvettes. CoOEP and MeOPy solution samples were prepared with analytical grade toluene and phenyloctane and gave similar extinction coefficient values. Spectra were collected at 22 °C.

Computational Methods: Computations are performed with periodic density functional theory (DFT) using Vienna Ab-initio Simulation Package (VASP)[40,41,] version 5.4.4. or with the program Gaussian 09.[42] The DFT calculations were performed using the B3LYP functional and the 6-311G(d,p) basis. All Gaussian calculations were made on single molecules in the gas-phase or in toluene using the SCRF model with the SMD option.

The VASP code uses the projector augmented wave (PAW) method[41,43] to describe the core electrons and valence–core interactions. We used optB88-vdW functional[44,45] with PAW potentials optimized for the PBE functional[46] for all calculations. The electronic wavefunctions are sampled using a Gamma (Γ) point in the irreducible Brillouin zone (BZ) using the Monkhorst and Pack (MP)[47] method. A plane wave cut off energy of 550 eV was used for all simulations. Methfessel–Paxton smearing was used to set the partial occupancies for each wave function with a smearing width of 0.2 eV. All the geometries were fully optimized up to ~0.001 eV energy convergence. The choice of our DFT methodology, plane wave cutoff energies and k-point choice was based on previous periodic DFT simulations of similar systems of type[24,48-51] and size.[52] Additional computational details are presented in section 1 of the electronic supplementary information (ESI). VASP calculations were performed on species adsorbed to 2-layer graphite and on the same species in the gas phase.

RESULTS AND DISCUSSION

Binding of MeOPy to CoOEP in toluene solution.

Ligand affinity is quantitatively expressed by an experimentally measured equilibrium constant or, equivalently free energy difference between the bound and free states of the system calculated from the equilibrium constant. Previous equilibrium binding studies of different nitrogeneous bases to Co(II) porphyrins in solution have reported that these metal complexes tend to form five- and six-coordinate systems.[32-34] Furthermore, the formation (or stability) constants, K_s, for the five-coordinate complexes were found to be significantly larger than K_s for the cobalt porphyrins bound to two ligands. Pyridine based ligands are known to predominantly form penta-coordinate Co(II) porphyrin complexes.[34]

The binding affinity studies of MeOPy to CoOEP in solution as a function of ligand concentration were carried in toluene under ambient conditions. Because five-coordinate amine cobalt porphyrin adducts do not bind oxygen in solution at room temperature, inert environment was not necessary.[32] The titration experiments were followed by UV-visible absorption spectroscopy and the resulting spectral data are depicted in Figure 2. Increasing the solution concentration of MeOPy, produced a decrease in the intensity of the CoOEP Soret band at 394.5 nm, and Q bands at 553 nm, along with a concurrent appearance of a new peak at 422 nm. Clear isobestic points were observed at 403 and 542.5 nm (see Figure S2 in the ESI for more details) until the concentration of the ligand reached approximately 0.1 M confirming the formation of a stoichiometric, 1:1 MeOPy to CoOEP adduct. Above 0.1 M MeOPy solution concentration, at which the ligand to porphyrin ratio is greater than 10^4:1, a nonisosbestic trend developed in the titration spectra. Similar solution equilibria trends were reported for the spectroscopic titration of tetra(p-methoxyphenyl)porphinatocobalt(II), Co(*p*-OCH_3)TPP with different pyridine based ligands.[32] Here, the nonisosbestic behavior (which also occurred near 0.1 M in amine) was

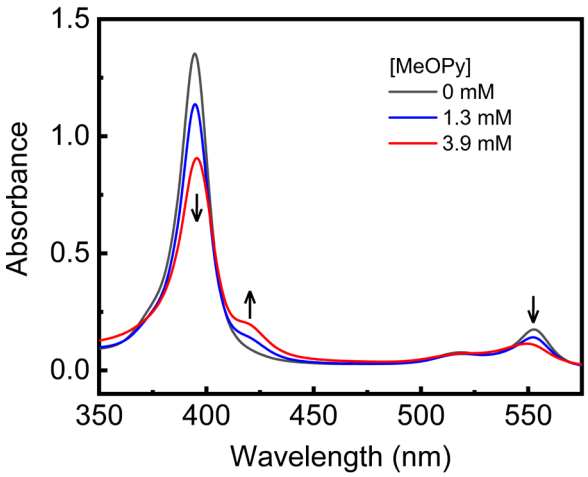

Figure 2. Overlaid absorption spectra of 5.0 x10^{-6} M CoOEP in toluene with coadded MeOPy ranging in concentration from 0 to 3.9 mM. Spectra were recorded at room temperature. Arrows indicate the direction of spectral changes with the addition of different amounts of the MeOPy ligand.

attributed to the formation of molecular complexes between the aromatic amine and the π-system of the porphyrin.[32]

For the complexation reaction:

$$\text{MeOPy} + \text{CoOEP} \rightleftarrows \text{MeOPy–CoOEP} \qquad (1)$$

the stability constant, K_s, defined as

$$K_s = \frac{[MeOPy{-}CoOEP]}{[CoOEP][MeOPy]} \qquad (2)$$

was determined by fitting the change in the absorption maxima at 394.5 nm in Figure 2 as

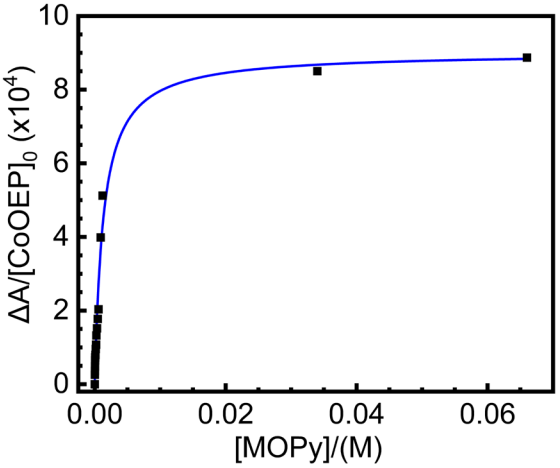

Figure 3. Change in the absorbance at 394.5 nm plotted as a function of variable MeOPy concentration added to 5.0 x 10^{-6} M CoOEP in toluene (black data points). Line (solid blue) indicates best fit for formation of the 1:1 MeOPy–CoOEP complex.

function of the concentration of MeOPy added using a non-linear curve fitting algorithm.[53] A similar fitting method was used to determine the equilibrium constant for the ligation of ZnTDP by 3-nitropyridine in *n*-tetradecane solution.[27] As in the case of MeOPy-CoOEP system, a decrease in intensity and a nominal red shift of the zinc porphyrin Soret band was observed with increasing nitro pyridine ligand concentration.[27]

The total absorbance measured at 394.5 nm in Figure 2 is equal to the sum of absorbance of the parent porphyrin and the absorbance of the ligated complex:

$$A_{total} = A_{CoOEP} + A_{MeOPy-CoOEP} \quad (3)$$

The observed change in absorbance is defined as:

$$\frac{\Delta A}{[CoOEP]_0} = \Delta\varepsilon \frac{K[MeOPy]}{1+K[MeOPy]} \quad (4)$$

where Δε is the difference in extinction coefficient between the porphyrin's complex state and $[CoOEP]_0$, the initial concentration of CoOEP (additional details of the fitting process can be found in the ESI). By applying Equation 4 to the absorbance data in Figure 2 one obtains a very satisfactory fit for the formation of the 1:1 five coordinate porphyrin complex. This fit is represented by the solid line in the graph in Figure 3. The calculated stability constant for the MeOPy:CoOEP system is 890 ± 65 M^{-1}, a value comparable to K_s for other cobalt porphyrins coordinated to a single pyridine based ligand.[32,33]

Using the relationship, $\Delta G_{soln} = -RTlnK_s$, the standard free energy of −16.8 ± 0.2 kJ/mol was calculated for the formation of the MeOPy:CoOEP complex at 298 K. This free energy value is comparable to the ΔG_{soln} quantities of −15.3 ± 0.2 kJ/mol and −16.5 ± 0.2 kJ/mol reported for Co(p-OCH_3)TPP complexed to a single pyridine and 4-methylpyridine ligand, respectively.[32,33] For pyridine ligated to Co(II)tetraphenylporphyrin, CoTPP, in toluene solution, ΔG_{soln} corresponded to −15.3 kJ/mol.[53] In general, the magnitude of the free energy parallels ligand bond strength or ligand affinity. For nitrogenous bases, the ligand bond strength has been shown to increase with the increasing basicity (or pK_a) of the ligand. Thus, by comparing pK_a values for pyridine (5.22), 4-methylpyridine (5.98) and MeOPy (6.58) it is clear that MeOPy is most basic in this series and is expected to have the highest binding affinity. This is supported by the trend in the ΔG_{soln} values for these ligands.[32,33]

Binding of MeOPy to CoOEP at phenyloctane/HOPG interface.

1. Ligand concentration dependence.

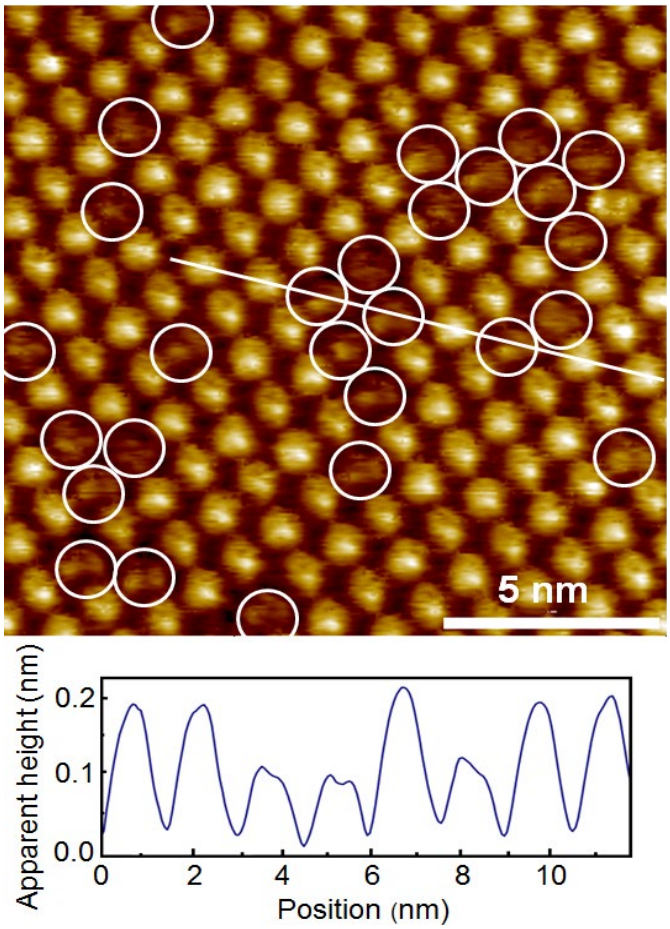

Figure 4. STM image of equal volumes of 1 x10^{-5} M of CoOEP after addition of 5 x 10^{-4} M acquired at the phenyloctane/HOPG interface. The constant current imaging was performed at room temperature under Ar with +500 mV bias and 20 pA setpoint. The white circles indicate ligated CoOEP/HOPG molecules. Cross-sectional profile is shown below the image.

All STM experiments investigating the binding of MeOPy to CoOEP were carried out in argon atmosphere to eliminate a possible interference of molecular oxygen which has been shown to readily bind to CoOEP at the octyl-benzene/HOPG interface.[22] Initially, 10 µL of 20 µM cobalt porphyrin in phenyloctane was added to a STM solution cell holding the HOPG substrate. After verifying that the substrate surface was uniformly covered with a monolayer of the porphyrin, a varied concentration of MeOPy ligand in phenyloctane (10 µL volume) was introduced to the STM solution cell and mixed gently with a pipette tip. The sample was allowed to equilibrate for 20 minutes before imaging. Based on the binding of MeOPy to CoOEP in solution (Figure 2), the lowest concentration of the ligand added was 10 times greater than that of metal porphyrin in order to assure observation of surface MeOPY-CoOEP complexes.

Figure 4 represents a typical STM image for CoOEP at the phenyloctane/HOPG interface at room temperature after addition of a 5 x 10^{-4} M MeOPy solution. Here, two types of features are readily identified: bright and dim (circled white). The unligated CoOEP molecules are recognized as the bright features due to electron tunneling through the half-filled d_{z2} orbitals of the cobalt ions.[54] The dim spots are assigned to the MeOPy-CoOEP coordinated species. The cross-sectional profile in Figure 4, emphasizes the difference between the ligated and unbound molecules. The low conductivity of ligated cobalt cores is due to the MeOPy lack of electronic states near the Fermi level that attenuate the signal and allow differentiation between the ligated and unligated species in STM images. Similar tunneling contrast was observed in images CoOEP was bound to molecular oxygen at the phenyloctane/HOPG interface where the coordinated cobalt centers appeared dim.[22]

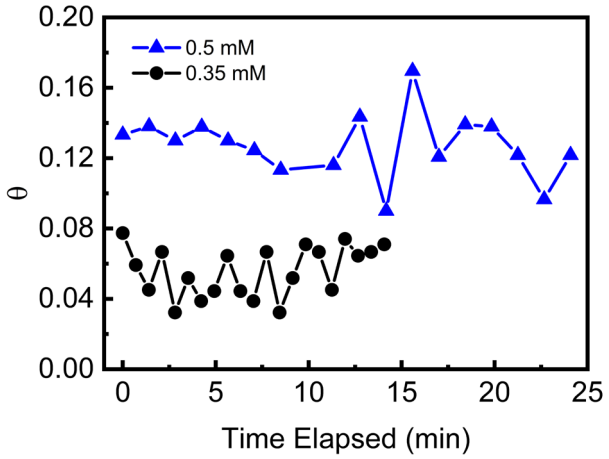

Figure 5. Variation of θ with time when the solution concentration of MeOPy concentration is $3.5x10^{-4}$ M (black trace) and $5.0x10^{-4}$ M (blue trace). STM images for this data were collected sequentially over a period of 9 and 25 minutes respectively at 22° C MeOPy. The respective average θ over these time periods are 0.07 ± 0.025 (black trace) and 0.13 ± 0.025 (blue trace).

To determine if the MeOPy ligation to CoOEP is a dynamic process, a series of consecutive scans were recorded for prolonged periods of time over the same sample area containing both bright and dark molecules (Figure S3 in the ESI). A 'blinking', i.e. vanishing and appearance of the dark molecules confirmed that the binding process was indeed reversible. Two sets of such consecutive image series where the concentration of the MeOPy ligand varied were analyzed for potential system equilibration. Here, the surface coverage (θ) is defined as the number of bright molecules in an image (MeOPy–CoOEP) divided by the total number of CoOEP surface molecules. The data in Figure 5 were collected after the system had been allowed to come to equilibrium for 2 hours at 22 °C. The STM images analyzed contained about 225 surface CoOEP molecules. Clearly, there is exchange of MeOPy occurring between the solution and the surface supported CoOEP and the ligation process has reached equilibrium.

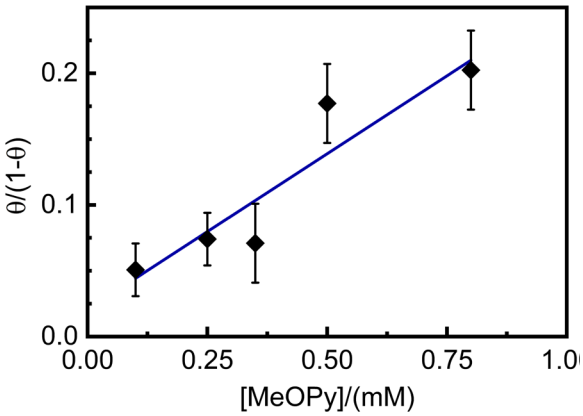

Figure 6. The quantity θ/(1-θ) plotted as a function of MeOPy concentration in the solution at 22° C. Error bars indicate ± 1 standard deviation.

For quantitative evaluation of the binding affinity of the MeOPy toward CoOEP/HOPG system, several of STM experiments were conducted where the concentration of the MeOPy ligand in solution varied from 0.1 mM to 0.8 mM. Using the previously defined θ, as the surface coverage of the MeOPy–CoOEP complex, we plotted the quantity θ/(1 – θ) as a function of the solution concentration of the MeOPy ligand (Figure 6). The equilibrium dtat for MeOPy binding to CoOEP can be fit the Langmuir adsorption model which assumes a single binding events and a maximum binding capacity corresponding to monolayer surface coverage.

The Langmuir equilibrium constant for MeOPy binding to CoOEP/HOPG in solution can be written as

$$K_c = \frac{\theta}{(1-\theta)(c/c^0)} \qquad (5)$$

where c_0 is taken the solution standard state of 1 M MeOPy and the standard state coverage is 0.5. The slope of the line in Figure 6 provides the value of K_c which then can be used to calculate the change in the free energy. For the current system one arrives at ΔG_c(295 K) of −13.0 ± 0.3 kJ/mol.

2. Temperature Dependence.

To obtain the remaining thermodynamic functions additional STM data was collected from ligand binding experiments at temperatures of 15° C, 30 °C and 45 °C (Figure 7). Thermodynamic values, ΔS_c and ΔH_c were determined from a linear curve fit of ΔG_c as a function of temperature, Figure 8. Using the definition for entropy as, $\Delta S_c = -\left(\partial G/\partial T\right)_c$ and the change in enthalpy as, $\Delta H_c = \Delta G_c + T\Delta S_c$ one obtains the values
ΔS_c = −120 ± 17 J/mol·K and ΔH_c = −50 ± 5 kJ/mol for these state functions. The large

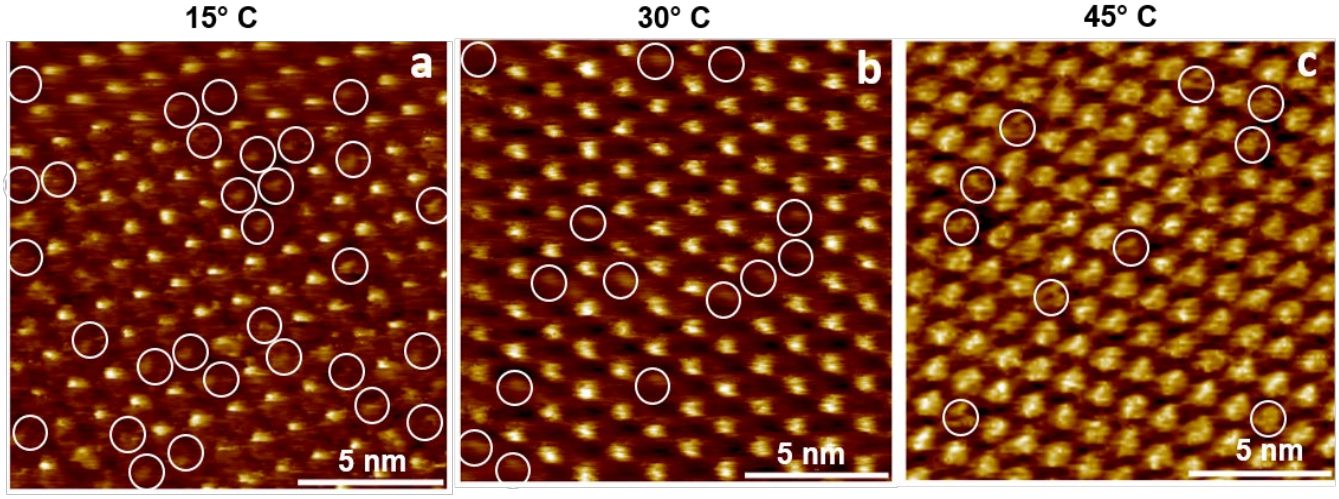

Figure 7. Representative STM images collected in constant current imaging mode of MeOPy binding to CoOEP at the phenyloctane/HOPG interface at different temperatures (a) 15° C, (b) 30° C and (c) 45° C. Imaging conditions were (a) +400 mV bias and 15 pA setpoint, (b) -600 mV, 30 pA, (c) -600 mV, 35 pA.

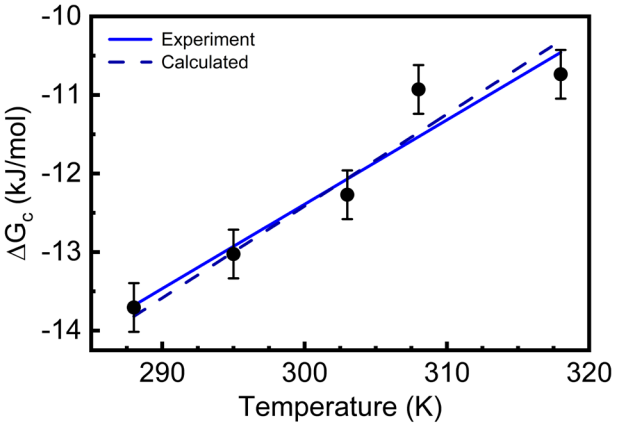

Figure 8. ΔG_c plotted as a function of temperature. The solid line represents a best fit of the experimental data where the slope 120 J/mol is the measured ΔS_c relative to 1 M MeOPy standard state. The dashed line is shown with a slope equal to ΔS_c calculated through statistical mechanics, –116 J/K mol.

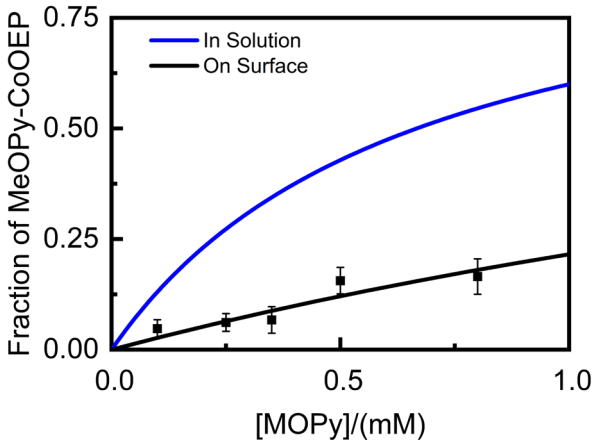

Figure 9. Comparison of the fraction of ligated CoOEP plotted against the initial concentration of MeOPy in solution (blue line) and adsorbed onto HOPG (black line). The ligand affinity data in solution is based by electronic spectroscopy. The fraction of ligated CoOEP/HOPG molecules was determined from STM imaging experiments.

negative entropy change is due to the loss of translational and rotational degrees of freedom by the ligand–porphyrin complex absorbed on the surface. For comparison, the change in the entropy was derived from statistical mechanics.[22,24,55] The calculated value of ΔS_c is –116 J/mol·K mol and was used as the slope of the dashed line in Figure 8. The y-intercept of that line is ΔH_c, with a value of –47 kJ/mol.

The experimental free energy value for the ligation reaction of MeOPy to CoOEP in solution (-16.8±0.2 kJ/mole) is more negative than the ΔG for cobalt porphyrin complexed at the solution/HOPG interface (–13.0±0.3 kJ/mol), This is also the case for the computed values (Table 1). We infer that the ligand binding affinity of the metalloporphyrin is higher in a solvent than when CoOEP is bound to the HOPG substrate (Table 1). This marked difference in the ligand affinity is depicted graphically in Figure 9. The fraction of MeOPy-CoOEP formed on the surface is less than half the fraction of the ligated complex formed in solution under the same MeOPy and CoOEP stoichiometric conditions, with the MeOPy to CoOEP ratios ranging from 10:1 to 100:1. This result indicates that the MeOPy interacts more strongly with the CoOEP in solution than porphyrin receptors on a surface.

The DFT calculated thermodynamic values (Table 1 and section 1 of the ESI) are in excellent agreement with experiment considering the relatively low level of theory used. Perhaps most importantly theory predicts that the surface bound MeOPy should be less stable than the same species in solution – as is observed.

Table 1. Experimental and calculated thermodynamic values for the formation of a five coordinate MeOPy–CoOEP complex at 298 °C.

System	$K_{s(c)}$ (M^{-1})	ΔG (kJ/mol)		ΔH (kJ/mol)		ΔS (J/Kmol)	
	Exp.	Exp.	Calc.	Exp.	Calc.	Exp.	Calc.
MeOPy–CoOEP (sol.)	890	-16.8±0.2	-23		-58		-114
MeOPy–CoOEP (HOPG)	190	-13.0±0.3	-20	-50±5	-55	-120±17	-117

A different competition for ligand binding was reported when HOPG was exposed to premixed *n*-tetradecane solutions of 3-nitropyridine, NO_2Py and ZnTDP.[27] Although the measured formation constant for NO_2Py–ZnTDP in solution was very large ($2.0\pm0.5 \times 10^4$ M^{-1}), STM images revealed that the percentage of bound surface molecules was greater than the percentage in solution.[27] Thus, NO_2Py binds more strongly to surface supported ZnTDP than it does to ZnTDP in solution.

3. High ligand concentration induced desorption of CoOEP from HOPG

Low affinity binding in solution implies that a relatively high concentration of the MeOPy ligand is required before the maximum binding to CoOEP on the surface is achieved. At ligand concentrations below about 0.8 mM, the number of bound porphyrin sites on HOPG scales roughly linearly with increasing concentration of MeOPy (Figure 6) with the CoOEP monolayer remaining intact. However, when the concentration of MeOPy is increased above 1 mM (i.e. 100 times the concentration of CoOEP), significant desorption of the molecular monolayer (about 20%) at the grain boundaries and within the monolayer itself is observed. Figure 10 shows STM images of an intact porphyrin monolayer and a partially disrupted monolayer. The depleted monolayer does not reconstruct or heal with scanning time. The same surface monolayer coverage trend was observed in STM experiments when premixed solutions containing similar ratios of the MeOPy and CoOEP as in sequential depositions were employed (Figure S4 in the ESI).

The above results are very surprising because previous STM studies of CoOEP at the phenyloctane/HOPG (or Au) interface showed that the porphyrin monolayer is quite stable and does not do not desorb from the substrate until about 70 °C.[56-58] A possible explanation for the loss of monolayer from the HOPG surface, is that it forms a soluble six coordinate porphyrin complex at high MeOPy concentrations.

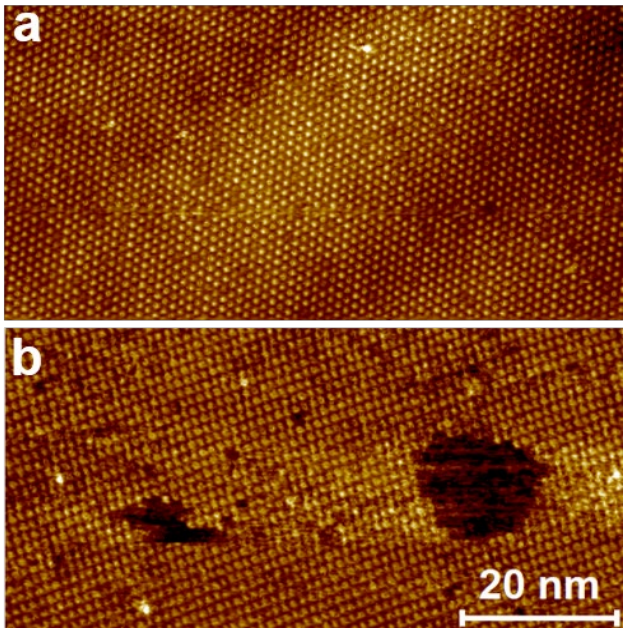

Figure 10. Low resolution 40 x 80 nm STM images comparing two different ratios of MeOPy and CoOEP ratios at the phenyloctane/HOPG interface (a) 35:1 and (b) 100:1. Images were acquired under inert atmosphere at 22° C; -500 mV and (a) 25 pA, (b) 20 pA.

Desorption from grain boundaries and defects is much faster than from within the monolayer and once the MeOPy–CoOEP or CoOEP complex desorbes it might be converted to the 6-coordinates species that does not form an ordered monolayer. This is less likely for the MeOPy–CoOEP complex for two reasons. First, pyridine based ligands mostly form penta-coordinate cobalt porphyrin complexes. Second, an MeOPy to CoOEP ratio greater than 10^4:1 is required for the formation of a six coordinate complex in solution.[32] Under the conditions where loss of monolayer is first observed, the MeOPy ligand concentration is only 200 times that of the CoOEP.

An alternative explanation might be that the MeOPy-CoOEP complex desorbs more easily from HOPG than the parent CoOEP complex. In order to test this, we performed density functional calculations to determine the desorption energies both in UHV and in solution (details of the calculations are presented in the ESI).

Table 2. DFT calculated desorption energies for indicated complexes in gas phase and in toluene solution.

System	ΔH_{vap} kJ/mole	ΔH_{sln} kJ/mole
CoOEP/HOPG	373	240
MeOPy–CoOEP/HOPG	383	237

The enthalpy change for the gas phase desorption reaction, Equation 6, at zero K is simply the electronic energy difference as computed by VASP. With the assumption that the internal energies of the HOPG and CoOEP do not change with desorption, the change in enthalpy is the change in zero point energy plus 3RT. This result and the related one for Equation 7 are given in Table 2.

CoOEP/HOPG ⇄ CoOEP + HOPG (6)

MeOPy-CoOEP/HOPG ⇄ MeOPy-CoOEP + HOPG (7)

The calculation in solution requires accounting for immersion of the reactants and products in solvent. The heat of immersion of CoOEP is a direct result of our Gaussian calculations (see ESI section 1). The heat of immersion of CoOEP/HOPG was determined using the solvent accessible area of the surface supported species and the computed heat of immersion of CoOEP (see Supplementary Information for details).[59] A similar calculation was performed for MeOPy-CoOEP/HOPG. The heat of immersion of HOPG in toluene was also calculated using Gaussian in order to keep a consistent model throughout. To do this a 2-layer slab of HOPG was hydrogen terminated to make the super-molecule $C_{164}H_{48}$ and the same SCRF(SMD) procedure was used to determine the heat of immersion. This heat of immersion (–256 kJ/mole) was then multiplied by the ratio of the effective area per porphyrin divided by the area of carbon in the supermolecule in order to obtain the heat of immersion of HOPG per mole of porphyrin (-97 kJ/mole – porphyrin).

The resulting solution phase desorption energies,

$\Delta H_{sln} = \Delta H_g + \Delta H_I(HOPG) + \Delta H_I(porphyrin) - \Delta H_I(porphyrin/HOPG)$ (8)

are given in Table 2.

Although the VASP computed desorption energies are probably an overestimate and they are significantly reduced by the effects of solvation, they are clearly very similar in size. The values in Table 2 are probably too high since it is known from previous experiments,[56,57] that the activation energy for desorption is 125 kJ/mole for CoOEP/HOPG in phenyloctane[5858]. We note, however, that thermodynamic desorption energies should be smaller than the desorption activation energy.[60] The important result here is that the desorption energy for MeOPy-CoOEP is very close to that of CoOEP and is quite large. Thus, it seems unlikely that a preferential desorption of MeOPy–CoOEP is responsible for the loss of the monolayer.

A third origin for the monolayer dissolution may lay in the proposal offered by Walker for nonisosbestic behavior of the absorption spectra of related complexes.[32] Aggregation of ligand molecules about the porphyrin ring may somehow inhibit the formation of an ordered monolayer (once a complex has desorbed from a grain boundary or defect). Such aggregation onto the adsorbed complex might also significantly lower the desorption energy. While this is occurring at about $1/10^{th}$ the concentration where it is clearly seen in the absorbance spectrum, there may be more than one possible aggregate structure. It is also possible that the residence time of MeOPy on HOPG is long enough that at high concentrations it effectively blocks return of the porphyrin to the HOPG surface. Interestingly, the dissolution effect is reduced with increasing temperature.

Experiments are currently underway to better understand the driving cause(s) for the desorption of MeOPy–CoOEP from the graphite surface.

4. Cooperativity

Electronic communication between the substrate and the adsorbed porphyrin can influence the receptor's affinity toward an exogenous ligand. Possible cooperativity operating between adjacent CoOEP receptors on HOPG and the MeOPy ligands was examined by inspecting the distribution of dark molecules (ligated molecules) in the cobalt porphyrin monolayer and comparing the result with calculated random distribution. The details of the nearest neighbor analysis are provided in the Supplementary Information along with a representative STM image (Figure S5) that identifies the different grouping of the MeOPy–CoOEP surface species. In Figure 11, the experimental distribution (orange bars) was determined by counting the number of adjacent molecules that are ligated. Images that showed 15% surface ligated species were used in this analysis for a total of nearly 4000 molecules counted. The random distribution was modeled by a binomial distribution, green bars in Figure 11, for the case when θ = 15%. The random distribution simulates the case where there is no preference for MeOPy binding to adjacent CoOEP molecules. If the distribution of dark nearest neighbors was random, we would expect the calculated fractions to equal to the experimentally determined fraction of MeOPy–CoOEP. This, however, is not what we observe. Comparing the experimental and random distributions we see an increase in the numbers of pairs and larger groupings of three and four of molecules for the experimental set. This result suggests that the binding of MeOPy to a given CoOEP molecule on HOPG substrate increases the chance that another MeOPy will bind to a neighboring molecule in the monolayer – an indication of surface mediated positive cooperativity.

It is important to note that the coverage represented by Figure 11 is at the extreme end of the data used to derive the Langmuir equilibrium constant. Cooperativity, therefore, is playing only a small role in the data used in Figure 8 and the corresponding analysis. The concentration region where cooperativity would play a significant role is the same region where the monolayer begins to dissolve.

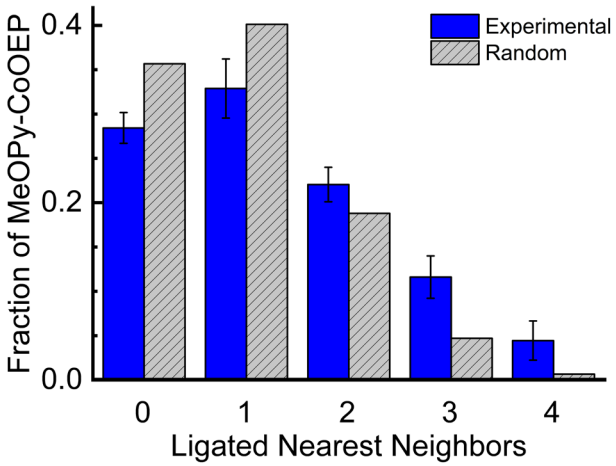

Figure 11. Histogram comparing the theoretical distribution of dark nearest neighbors (for p = 0.156) and experimentally observed distribution for ligand-bound molecules in bar diagrams of nearest-neighbor distributions of MeOPy bound CoOEP molecules: gray, random distribution; solid blue, distribution as measured in the STM images. N = 3990 molecules. Error bars are standard error of mean.

CONCLUSION

In this work we have shown that MeOPy binds to CoOEP adsorbed on HOPG and when dissolved in fluid solution. The coordination of the ligand to CoOEP adsorbed on HOPG at low MeOPy concentration followed a simple Langmuir adsorption isotherm. Contributions of free energy, enthalpy and entropy to the binding process on the surface and in solution were experimentally determined and computationally estimated. Both methods are in satisfactory agreement. The free energy value for the ligation reaction of MeOPy to CoOEP/HOPG at the solution interface, −13.0±0.3 kJ/mol, is less negative than the ΔG for cobalt porphyrin complexed in solution, −16.8±0.2 kJ/mol, leading us to conclude that the ligand binding affinity of the metalloporphyrin is higher in solution than when CoOEP is bound to the HOPG substrate.

Increasing the concentration of MeOPy to 100

times that of the CoOEP receptor initiates a significant desorption of the molecular monolayer at the grain boundaries and within the monolayer itself. The depleted monolayer does not reconstruct or heal with scanning time, although there are obvious changes in shape of the bare areas. The same surface monolayer coverage trend was observed in STM experiments where premixed solutions containing similar ratios of the MeOPy and CoOEP as in cases where sequential depositions were employed. At this time, we speculate that dissolution of the molecular monolayer may be due to solvation of the five-coordinate pyridinate complex and/or the CoOEP complex by excess pyridine.

At higher concentrations of MeOPy, the distribution of ligated porphyrins in the CoOEP/HOPG monolayer shows a preference for MeOPy binding in groups of two or more indicating that the CoOEP receptors' reactivity is moderated by the HOPG substrate in a way that leads to positive cooperativity.

Computational studies based on density functional methods were used to determine ΔS and DH values for the solution and surface reactions that were in very good agreement with experiment. The agreement between measured and computed changes in free energy are good, but the computed values are too large. They do show the appropriate trend – The DG for reaction at the surface is not as negative as that for the reaction in solution.

AUTHOR INFORMATION

Corresponding Author

umazur@wsu.edu; hipps@wsu.edu

ORCID

Kristen Johnson: 0000-0003-3622-9686

K. W. Hipps: 0000-0002-5944-5114

Ursula Mazur: 0000-0002-3471-4883

CONFLICTS OF INTEREST

The authors declare no competing financial interest.

ACKNOWLEDGMENT

This material is based upon work supported by the National Science Foundation under grant CHE-1800070. We gratefully acknowledge their support.

FOOTNOTE

†Electronic Supplementary Information (ESI) is available. Included are the details of the DFT calculations for the equilibrium thermodynamic data for the binding of MeOPy–CoOEP and for the desorption energies; additional STM images of the MeOPy binding process; nearest neighbor analysis of cooperative ligand binding. See DOI:

REFERENCES

1 K. Wheelock, J. J. Zhang, R. McConnell, D. Tang, H. E. Volk, Y. Wang, J. B. Herbstman, S. Wang, D. H. Phillips, D. Camann, J. Gong and F. Perera, *Environ. Sci. Process. Impacts*, 2018, **20**, 780–789.

2 L. Huang, Q. Shuai and S. Hu, *J. Clean. Prod.*, 2019, **215**, 280–289.

3 K. M. Kadish, K. M. Smith and R. Guilard, in *Handbook of Porphyrin Science With Applications to Chemistry, Physics, Materials Science, Engineering, Biology and Medicine — Volume 26: Heme Biochemistry*, ed. G. C. Ferreira, World Scientific Publishing Company, Singapore, 2013, vol. 26.

4 A. R. Smith and J. Klosek, *Fuel Process. Technol.,* 2001, **70**, 115–134.

5 Z. Zhao-Karger, P. Gao, T. Ebert, S. Klyatskaya, Z. Chen, M. Ruben and M. Fichtner, *Adv. Mater.*, 2019, **31**, 1806599.

6 R. Paolesse, S. Nardis, D. Monti, M. Stefanelli and C. Di Natale, *Chem. Rev.*, 2016, **117**, 2517–2583.

7 A. Robertson and S. Shinkai, *Coord. Chem. Rev.*, 2000, **205**, 157–199.

8 I. Batinic-Haberle, A. Tovmasyan and I. Spasojevic, *Antioxidants Redox Signal.*, 2018, 29, 1691–1724.

9 R. Khan, M. Özkan, A. Khaligh and D. Tuncel, *Photochem. Photobiol. Sci.*, 2019, **18**, 1147–1155.

10 S. Nakagaki, G. K. B. Ferreira, G. M. Ucoski and K. A. D. De Freitas Castro, *Molecules*, 2013, **18**, 7279–7308.

11 J. C. Barona-Castaño, C. C. Carmona-Vargas, T. J. Brocksom, K. T. De Oliveira, M. Graça, P. M. S. Neves, M. Amparo and F. Faustino, *Molecules*, 2016, **21**. DOI: 10.3390/molecules21030310

12 A. Bellelli and J. Carey, in *Reversible Ligand Binding: Theory and Experiment*, Wiley, Hoboken, NJ, 2017.

13 P. A. Gale and J. W. Steed, in *Supramolecular Chemistry: From Molecules to Nanomaterials*, Wiley, Hoboken, NJ, 2012, vol 8.

14 J. Otsuki, *Coord. Chem. Rev.*, 2010, **254**, 2311–2341.

15 J. M. Gottfried, *Surf. Sci. Rep.*, 2015, **70**, 259–379.

16 W. Auwärter, D. Écija, F. Klappenberger and J. V. Barth, *Nat. Chem.*, 2015, **7**, 105–120.

17 K. Seufert, W. Auwärter and J. V. Barth, *J. Am. Chem. Soc.*, 2010, **132**, 18141–18146.

18 K. W. Hipps and L. Scudiero, *J. Chem. Educ.*, 2005, **82**, 704–711.

19 A. M. Moore and P. S. Weiss, *Annu. Rev. Anal. Chem.*, 2008, **1**, 857–882.

20 Q. Li and Q. Lu, *Rev. Sci. Instrum.*, 2011, **82**, DOI:10.1063/1.3585200.

21 D. den Boer, M. Li, T. Habets, P. Iavicoli, A. E. Rowan, R. J. M. Nolte, S. Speller, D. B. Amabilino, S. De Feyter and J. A. A. W. Elemans, *Nat. Chem.*, 2013, **5**, 621–627.

22 B. A. Friesen, A. Bhattarai, U. Mazur and K. W. Hipps, *J. Am. Chem. Soc.*, 2012, **134**, 14897–14904.

23 Y. Hao, R. S. Weatherup, B. Eren, G. A. Somorjai and M. Salmeron, *Langmuir*, 2016, **32**, 5526–5531.

24 G. Nandi, B. Chilukuri, K. W. Hipps and U. Mazur, *Phys. Chem. Chem. Phys.*, 2016, **18**, 20819–20829.

25 J. Otsuki, E. Seki, T. Taguchi, M. Asakawa and K. Miyake, *Chem. Lett.*, 2007, **36**, 740–741.

26 Q. Ferreira, L. Alccer and J. Morgado, *Nanotechnology*, 2011, **22**, 435604.

27 J. Visser, N. Katsonis, J. Vicario and B. L. Feringa, *Langmuir*, 2009, **25**, 5980–5985.

28 U. Mazur and K. W. Hipps, *J. Porphyr. Phthalocyanines*, 2020, DOI: 10.1142/s1088424620300049

29 B. E. Murphy, S. A. Krasnikov, N. N. Sergeeva, A. A. Cafolla, A. B. Preobrajenski, A. N. Chaika, O. Lübben and I. V. Shvets, *ACS Nano*, 2014, **8**, 5190–5198.

30 B. Hulsken, R. Van Hameren, J. W. Gerritsen, T. Khoury, P. Thordarson, M. J. Crossley, A. E. Rowan, R. J. M. Nolte, J. A. A. W. Elemans and S. Speller, *Nat. Nanotechnol.*, 2007, **2**, 285–289.

31 J. M. Gottfried, *Surf. Sci. Rep.*, 2015, **70**, 259–379.

32 F. A. Walker, *J. Am. Chem. Soc.*, 1973, **95**, 1150–1153.

33 F. A. Walker, *J. Am. Chem. Soc.*, 1973, **95**, 1154–1159.

34 D. V. Stynes, H. Cleary. Stynes, B. R. James and J. A. Ibers, *J. Am. Chem. Soc.*, 2002, **95**, 1796–1801.

35 J. S. Summers, J. L. Petersen and A. M. Stolzenberg, *J. Am. Chem. Soc.*, 2002, **116**, 7189–7195.

36 A. Satake and Y. Kobuke, *Tetrahedron*, 2005, **61**, 13–41.

37 D. Delmarre and C. Bied-Charreton, *Sensors Actuators, B Chem.*, 2000, **62**, 136–142.

38 L. Ye, Y. Fang, Z. Ou, L. Wang, S. Xue, Y. Lu and K. M. Kadish, *J. Porphyr. Phthalocyanines*, 2019, **23**, 196–206.

39 K. B. Fields, J. T. Engle, S. Sripothongnak, C. Kim, X. P. Zhang and C. J. Ziegler, *Chem. Commun.*, 2011, **47**, 749–751.

40 G. Kresse and J. Furthmüller, *Comput. Mater. Sci.*, 1996, **6**, 15–50.

41 G. Kresse and D. Joubert, *Phys. Rev. B - Condens. Matter Mater. Phys.*, 1999, **59**, 1758–1775.

42 M. J. Frisch, G. W. Trucks, H. B. Schlegel, G. E. Scuseria, M. A. Robb, J. R. Cheeseman, G. Scalmani, V. Barone, B. Mennucci, G. A. Petersson, H. Nakatsuji, M. Caricato, X. Li, H. P. Hratchian, A. F. Izmaylov, J. Bloino, G. Zheng, J. L. Sonnenberg, M. Hada, M. Ehara, K. Toyota, R. Fukuda, J. Hasegawa, M. Ishida, T. Nakajima, Y. Honda, O. Kitao, H. Nakai, T. Vreven, J. A. Montgomery, Jr., J. E. Peralta, F. Ogliaro, M. Bearpark, J. J. Heyd, E. Brothers, K. N. Kudin, V. N. Staroverov, T. Keith, R. Kobayashi, J. Normand, K. Raghavachari, A. Rendell, J. C. Burant, S. S. Iyengar, J. Tomasi, M. Cossi, N. Rega, J. M. Millam, M. Klene, J. E. Knox, J. B. Cross, V. Bakken, C. Adamo, J. Jaramillo, R. Gomperts, R. E. Stratmann, O. Yazyev, A. J. Austin, R. Cammi, C. Pomelli, J. W. Ochterski, R. L. Martin, K. Morokuma, V. G. Zakrzewski, G. A. Voth, P. Salvador, J. J. Dannenberg, S. Dapprich, A. D. Daniels, O. Farkas, J. B. Foresman, J. V. Ortiz, J. Cioslowski, and D. J. Fox, Gaussian 09 (Revision D.01), Gaussian, Inc., Wallingford CT, 2013.

43 P. E. Blöchl, *Phys. Rev. B*, 1994, **50**, 17953–17979.

44 J. Klime, D. R. Bowler and A. Michaelides, *Phys. Rev. B - Condens. Matter Mater. Phys.*, 2011, **83**, 195131.

45 A. D. Becke, *Phys. Rev. A*, 1988, **38**, 3098–3100.

46 J. P. Perdew, K. Burke and M. Ernzerhof, *Phys. Rev. Lett.*, 1996, **77**, 3865–3868.

47 H. J. Monkhorst and J. D. Pack, *Phys. Rev. B*, 1976, **13**, 5188–5192.

48 A. Jahanbekam, B. Chilukuri, U. Mazur and K. W. Hipps, *J. Phys. Chem. C*, 2015, **119**, 25364–25376.

49 B. Chilukuri, U. Mazur and K. W. Hipps, *Phys. Chem. Chem. Phys.*, 2014, **16**, 14096–14107.

50 B. Borders, M. Adinehnia, B. Chilukuri, M. Ruf, K. W. Hipps and U. Mazur, *J. Mater. Chem. C*, 2018, **6**, 4041–4056.

51 M. Adinehnia, B. Borders, M. Ruf, B. Chilukuri, K. W. Hipps and U. Mazur, *J. Mater. Chem. C*, 2016, **4**, 10223–10239.

52 Y. C. Zhang, B. Chilukuri, T. B. Hanson, Z. M. Heiden and D. Y. Lee, *J. Phys. Chem. Lett.*, 2019, **10**, 3525–3530.

53 H. Tsukube, H. Furuta, A. Odani, Y. Takeda, Y. Kudo, Y. Inoue, Y. Liu, H. Sakamoto and K. Kimura, in *Comprehensive Supramolecular Chemistry, Volume 8: Physical Methods in Supramolecular Chemistry*, ed. J. E. D. Davies, and J. A. Ripmeester, Pergamon, Tarrytown, NY, 1st edn., 1996, vol. 8. pp. 425-441.

54 L. Scudiero, D. E. Barlow and K. W. Hipps, *J. Phys. Chem. B*, 2001, **106**, 996–1003.

55 M. Mammen, E. I. Shakhnovich, J. M. Deutch and G. M. Whitesides, *J. Org. Chem.*, 1998, **63**, 3821–3830.

56 A. Bhattarai, U. Mazur and K. W. Hipps, *J. Am. Chem. Soc.*, 2014, **136**, 2142–2148.

57 A. Bhattarai, U. Mazur and K. W. Hipps, *J. Phys. Chem. C*, 2015, **119**, 9386–9394.

58 A. Bhattarai, K. Marchbanks-Owens, U. Mazur and K. W. Hipps, *J. Phys. Chem. C*, 2016, **120**, 18140–18150.

59 S. Conti and M. Cecchini, *Phys. Chem. Chem. Phys.*, 2016, **18**, 31480–31493.

60 K. W. Hipps and U. Mazur, *Langmuir*, 2018, 34, 3–17.